Scripta Materialia 197 (2021) 113789

Contents lists available at ScienceDirect

Scripta Materialia

journal homepage: www.elsevier.com/locate/scriptamat

Modelling the effect of intrinsic radiation damage on mechanical properties: The crystalline-to-amorphous transition in zircon

Norbert Huber[a,b,*], Tobias Beirau[c]

[a] Institute of Materials Mechanics, Helmholtz-Zentrum Geesthacht (HZG), 21502 Geesthacht, Germany
[b] Institute of Materials Physics and Technology, Hamburg University of Technology (TUHH), 21073 Hamburg, Germany
[c] Institute of Geosciences and Geography, Mineralogy/Geochemistry, Martin Luther University, Halle-Wittenberg, 06120 Halle, Germany

ARTICLE INFO

Article history:
Received 23 October 2020
Revised 26 January 2021
Accepted 5 February 2021
Available online 13 February 2021

Keywords:
Amorphization
Polyphase microstructure
Interfaces
Nanoindentation
Micromechanical modelling

ABSTRACT

Mechanical modelling using the level-cut Gaussian random field approach has been employed to simulate the effect of radiation induced amorphization on the Youngś modulus, Poissonś ratio and hardness of zircon ($ZrSiO_4$). A good agreement with previous nanoindentation experiments has been achieved. Two percolation transitions occur at ~16% and ~84% amorphous volume fraction, leading to deviations from linearity in the evolution of the Youngś modulus. Interface regions between crystalline and amorphous areas stabilise the hardness for a considerable amount of amorphous fraction. The modelling approach is promising for predicting the intrinsic radiation damage related evolution of the mechanical properties of various materials.

The mineral zircon (end-member composition $ZrSiO_4$, tetragonal structure, space group $I4_1/amd$) is in nature often exposed to nuclear radiation for millions of years, due to incorporated U and Th. Therefore, it has been found to be a suitable natural analogue for the study of the long-term behaviour of possible crystalline phases for nuclear waste disposal [1,2]. As the Zr-site can be completely replaced by actinides, e.g., Th, U, Np, Pu and Am [3–14], zircon itself has been proposed as a candidate crystalline host phase for the immobilization of actinides [10,15–17]. Recently, the isostructural end-member composition $USiO_4$ (coffinite) has been reported to be an important alteration product of UO_2 in spent nuclear fuel [18].

Intrinsic structural radiation damage is mainly caused by the α-decay of the incorporated actinides, see e.g. [19–22]. Most of the atomic displacements (several thousand per α-decay event) are induced by the heavy recoil nucleus, dissipating its energy by elastic collisions with surrounding atoms in its path through the structure. This generates recoil cascades in the ordered lattice that overlap and finally establish an amorphous (metamict) state. The smaller α-particle (helium nucleus) displaces only several hundred atoms near the end of its trajectory (major energy loss before by electronic excitations). The amorphization in, e.g., zircon goes along with significant swelling [9,23], a reduction of the density [19,24] and a measurable loss in modulus and hardness [25–27].

An elegant way for generating bi-continuous microstructures that have a percolation point at a defined phase volume fraction is established for foams [28] and nanoporous metals [29]. In these works, the method of levelled-cut random Gaussian fields [30,31] was used that allows for producing fully random as well as periodic structures. For such open pore materials, the considered range of the solid volume fraction ϕ_B is commonly limited to values below 50% and the percolation threshold ϕ_B^P above which a continuous 3D network is formed is around 10% [31]. Soyarslan et al. used FE-voxel models for the prediction of the macroscopic elastic properties and analysed the topology formed by the random Gaussian fields [29]. They determined the percolation threshold at $\phi_B^P = 15.9\%$. Symmetry implies that the second percolation threshold is $1 - \phi_B^P = 84.1\%$. In what follows, we apply the same method for generating a two-phase microstructure, where one phase is crystalline (ϕ_c) and the second phase is amorphous (ϕ_a) zircon. The latter undergoes swelling while being mechanically confined by the surrounding crystalline phase.

In this work we investigate whether mechanical modelling can confirm the results from earlier experiments and simulations of radiation-damaged zircon: (i) the radiation induced crystalline-to-amorphous transition can be properly described as a percolation problem with two percolation points [23,32,33], (ii) the Youngś modulus is threshold sensitive, and (iii) interfaces and underlying

* Corresponding author.
E-mail address: norbert.huber@hzg.de (N. Huber).

https://doi.org/10.1016/j.scriptamat.2021.113789

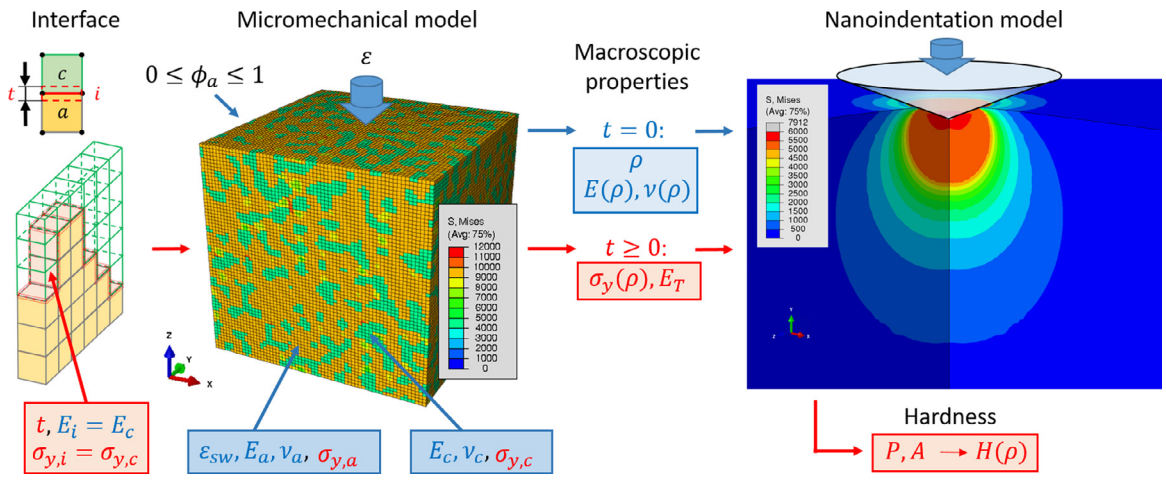

Fig. 1. Model for prediction of the mechanical properties for given phase composition and properties. RVE of the micromechanical model with optional interface of thickness t (left) used for homogenization of the mechanical properties after swelling; nanoindentation model (right) used for hardness prediction.

hard shells, enclosing the depleted amorphized cores, are able to stabilise the hardness [27,34].

The level-cut Gaussian random field modelling approach [29] defines the volumetric percolation points ϕ_a^{P1} and ϕ_a^{P2} at fixed values of 15.9% and 84.1%, respectively. ϕ_a^{P1} is very close to the predicted critical percolation density for a simple cubic lattice of 16.2% [35]. It should be noted that the associated critical percolation probability p_c is 0.31 [35], which has been reported to be in good agreement with p_{c1} of zircon [23,33]. The first percolation transition at ϕ_a^{P1} characterises the structural transition from islands of amorphous zircon within a matrix of crystalline zircon to a bi-continuous network of both phases at lower doses, whereas the second percolation transition ϕ_a^{P2} denotes the transition from the bi-continuous network to isolated islands of the remaining crystalline phase at higher doses. Beirau et al. found indications for the percolation transitions in the nanoindentation hardness and Young's modulus data as a function of density of natural zircon in agreement with the literature values [27,34].

Finite element simulations will be used to investigate the effect of the percolation points on the corresponding features arising in the mechanical properties. To this end, a two-scale simulation is established shown in Fig. 1 that allows for the simultaneous calibration of the material parameters of an elastic-plastic material law for crystalline and amorphous zircon, including the amount of swelling of the amorphous phase. The generation of the micromechanical model follows the approach of random Gaussian fields; see [29] for details. We use $H = \sqrt{146}$, which creates 96 independent directions for standing waves. A level cut of the superimposed waves with random phase shift decides to which phase the voxel is assigned at a given position. Mechanical properties are denoted with index a for the amorphous phase and c for the crystalline phase. The resulting FE model consists of 64 × 64 × 64 voxels and contains ~ 10 microstructural elements per edge length of the unit cell. At an amorphous fraction $\phi_a = 0.5$ this leads to a characteristic phase size that is 5% of the edge length of the model.

As an extension to [29], interface elements in form of 2D shell elements of thickness t are added to the surface of the amorphous phase, where t is defined as fraction of the voxel size. For a resolution of 64 voxels, an interface thickness of $t = 0.1$ corresponds to ~ 3% of the characteristic size of the crystalline phase ($\phi_a = 0.5$). Due to the volumetric overlap with the 3D HEX elements (Fig. 1, left), the added strength of the interface results from the product of the yield stress and the shell element thickness. The interface properties are chosen as the crystalline phase, e.g. $\sigma_{y,i} = \sigma_{y,c}$, while the shell element thickness is used as free parameter for calibrating the effective interface strength in the model. A compressive strain of 5% is applied in z-direction with periodic boundary conditions. For any phase volume fraction, the Representative Volume Element (RVE) allows to compute the macroscopic mechanical properties Young's modulus E, Poisson's ratio ν, yield stress σ_y, and work hardening rate E_T as function of the mechanical properties of the two phases.

The dependence of density, Young's modulus and hardness (loading along [100]) as function of dose is known for zircon from Sri Lanka (Ratnapura district) [19,26,27]. To determine the corresponding amorphous phase volume fraction ϕ_a an approximation is made, using the calibration scheme of [36,37]. These provide a reached maximum ϕ_a value of around 85% for the experiments of [26,27]. Rıós et al. [38] also propose a similar ϕ_a value for a sample with a comparable suffered radiation dose range. As long as the amorphous phase volume fraction is small, the swelling is constrained by the surrounding crystalline phase of high modulus and strength. Therefore, simulation step 1 applies swelling of the amorphous phase by the swelling strain ε_{sw}, which induces a volumetric swelling $V_{sw} = 3\varepsilon_{sw}$ in the unconfined condition. As initial value we use a swelling strain of $\varepsilon_{sw} = 6.7\%$ that corresponds to 18% volumetric swelling at 100% amorphization [39]. While ~ 13% swelling has found to be related to the recoil damage, the remaining ~ 5% are restricted to unit-cell swelling at low doses [32]. The latter is anisotropic, mainly affecting the c axis [19,40], hence the mechanical properties for uniaxial loading along [001]. For simplicity of our model, we assume that all swelling is isotropic and limited to the amorphized fraction.

For predicting the hardness, the Young's modulus and yield stress as determined from compression of the micromechanical model up to 5% strain (Fig. 1, left) are fed into the indentation simulation (Fig. 1, right). A linear work hardening with a work hardening rate of $E_T = 1$ GPa is applied, which does not affect the computed hardness. The rigid indenter is displaced by an indentation depth h at which the hardness $H = P/A$ is computed from the true contact area A by Abaqus, provided as field output variable contact area (CAREA) [41]. For details on the nanoindentation Finite Element model, we refer to [42].

The amorphous phase fraction before swelling $0 \le \phi_a \le 1$ is used for defining the structure of the micromechanical model. Examples displaying the evolution of the amorphous phase at characteristic stages are presented in Fig. 2. The elastic constants of both phases are tuned along the blue path in Fig. 1 by fitting the predicted macroscopic response of the RVE to the measured behaviour of Young's modulus versus density provided in [26,27]. With the

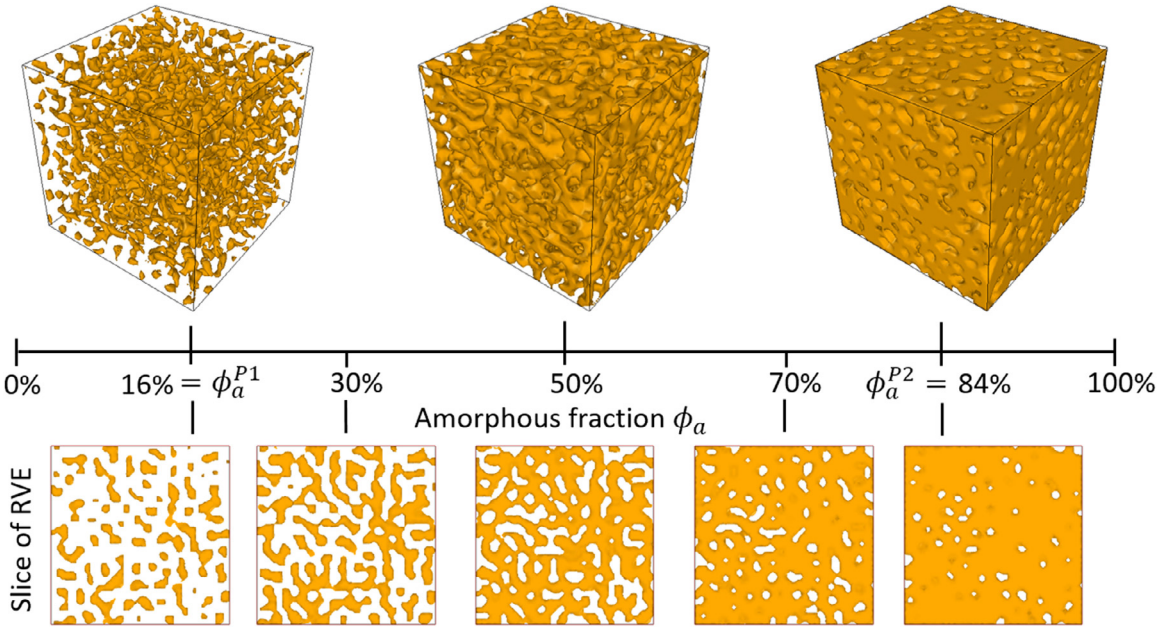

Fig. 2. Amorphous phase modelled with level-cut Gaussian random fields for increasing amorphous fraction ϕ_a. The crystalline phase is not shown. Images are visualised with OVITO [47].

Table 1
Calibrated material parameters of the phase constituents (assuming isotropic material behaviour) of the micromechanical model and resulting hardness values predicted by the indentation model.

Phase	E (GPa)	ν	σ_y (MPa)	E_T (MPa)	H (GPa)
Crystalline (c)	344.0	0.173	9131	1000	19.8
Amorphous (a)	129.9	0.281	4870	1000	10.4

calibration of the material parameters of the phase constituents assuming isotropic elastoplastic material behaviour as listed in Table 1, the dependency of $\rho(\phi_a)$ is finally achieved for a swelling strain of $\varepsilon_{sw} = 3.78\%$. The corresponding volumetric swelling is $V_{sw} = 11.5\%$ and thus $\sim 36\%$ less the experimentally observed total value [39], but very close to the $\sim 13\%$ swelling related to ϕ_a [32]. Further, our swelling value is in excellent agreement with that obtained by [43], using molecular dynamics simulations of zircon amorphized by melt-quenching (11%), while [44] report a somehow higher volume expansion (16%). It should be noted that melt-quenching may not truly represent the final amorphized state of a system. Irradiated systems may have a larger swelling than that of melt quenching [45,46].

Fig. 3 presents the results for the density and volumetric swelling as function of ϕ_a, where the open and solid symbols denote the data before and after swelling, respectively. Error bars from 10 realizations for amorphous fractions of 30, 50, and 70% show that the effect of the stochastic microstructure is negligible. The dependencies are only slightly changed by the swelling. Although the curves show some nonlinearity, which is a bit more pronounced for low amorphous fractions, no distinct features can be recognised that could be assigned to the percolation transitions. Nevertheless, it should be noted that [23] report a kink in the swelling rate to occur close to the percolation point. This is lesser obvious, but still visible in our modelled data as a slight increase in the slope around 16% ϕ_a.

Fig. 4 compares the predicted macroscopic mechanical properties versus the density of the composite material. The standard deviation of the macroscopic properties from 10 microstructure realizations of the RVE is $\sim 10^{-3}$ of the average value, which is why no error bars are shown for the simulation results. The overall good agreement of the predicted macroscopic Young's modulus E (green color) with the literature data (open symbols) indicates that the micromechanical model sufficiently approximates the microstructure and relevant phenomena of swelling and elastic deformation over the whole range of amorphous fractions. Although the resulting amorphous fraction of around 100% at densities just below 4.2 g/cm^3 seems at first glance somehow overestimated by the model, this is nevertheless in agreement with experimental data obtained for zircon [36,37] for doses $>7 \times 10^{18}$ α-events/g (dose-density correlation after [19]). Comparing the experimental density values [36,37] with that deduced from our model for the zircon samples from Beirau et al. [26,27] reveals a generally good agreement within the scatter and errors (only the sample with density ~ 4.54 g/cm^3 lies slightly below the corresponding region).

The predicted stiffness-density curve in Fig. 4 indicates the beginning deviation from a linear behaviour (tangents are added as dashed green curves) at both sides around ϕ_a^{P1} and ϕ_a^{P2}, providing evidence for the sensitivity of the Youngś modulus to the start of the percolation of the amorphous fraction and the end of the percolation of the crystalline fraction, respectively. Our model shows stronger deviation from linearity between $\sim 30\%$ and $\sim 70\%$ ϕ_a that seems to be pronounced enough to be also visible in the experimental data [27,34], despite the lower resolution and the higher uncertainty. This nonlinearity is in very good agreement with previous interpretation of the experimental data by Beirau et al. [27,34].

Compared to the Young's modulus, the Poisson's ratio shows a different behaviour with a maximum deviation from the secant drawn between the two end points (blue dashed line) at $\sim 70\%$ ϕ_a. While the predicted curve seems to deviate from the secant at the percolation transition ϕ_a^{P1} at low amorphous fractions, it shows an inflection at the percolation transition ϕ_a^{P2}. The agreement with the experimental data is very good for low amorphous fractions $\phi_a < 40\%$, whereas the experimental data are underpredicted between $40\% < \phi_a < 90\%$. Furthermore, the experimental curve exhibits an S shape, which saturates earlier than the simulation. This could be an indication that the microstructure generated with the level-cut Gaussian random field approach may

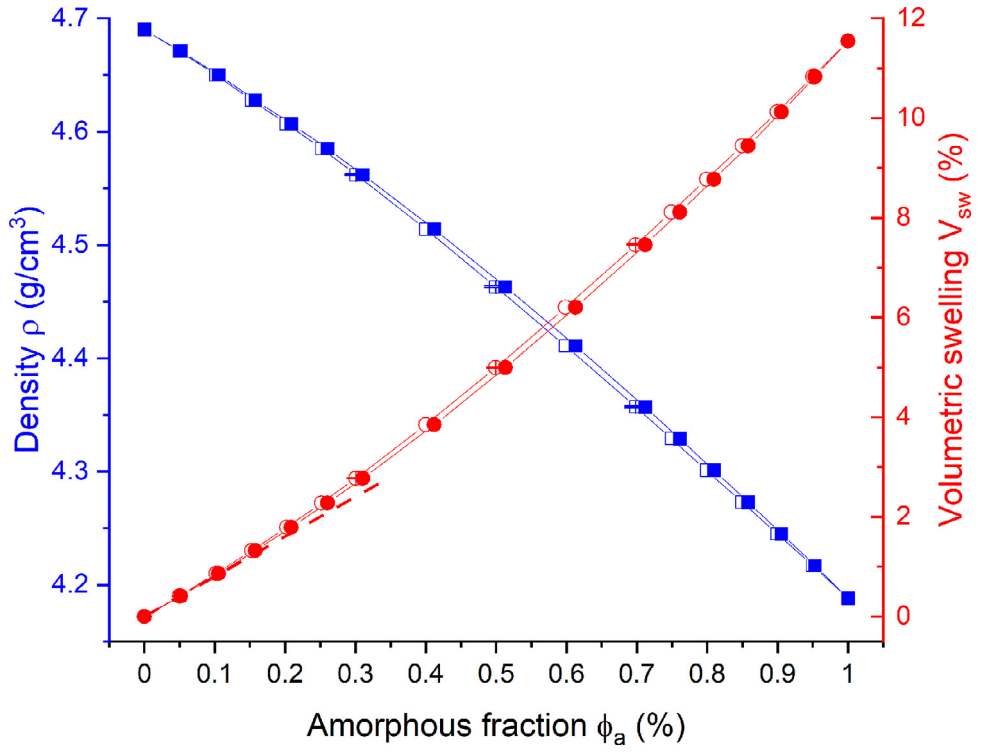

Fig. 3. Dependency of macroscopic volumetric swelling V_{sw} (red circles) and density ρ (blue squares) of the amorphous fraction ϕ_a (open symbols: initial values; solid symbols: after swelling of the amorphous phase). The swelling changes the macroscopic amorphous fraction only slightly. Data are available at [48]. (For interpretation of the references to color in this figure legend, the reader is referred to the web version of this article.)

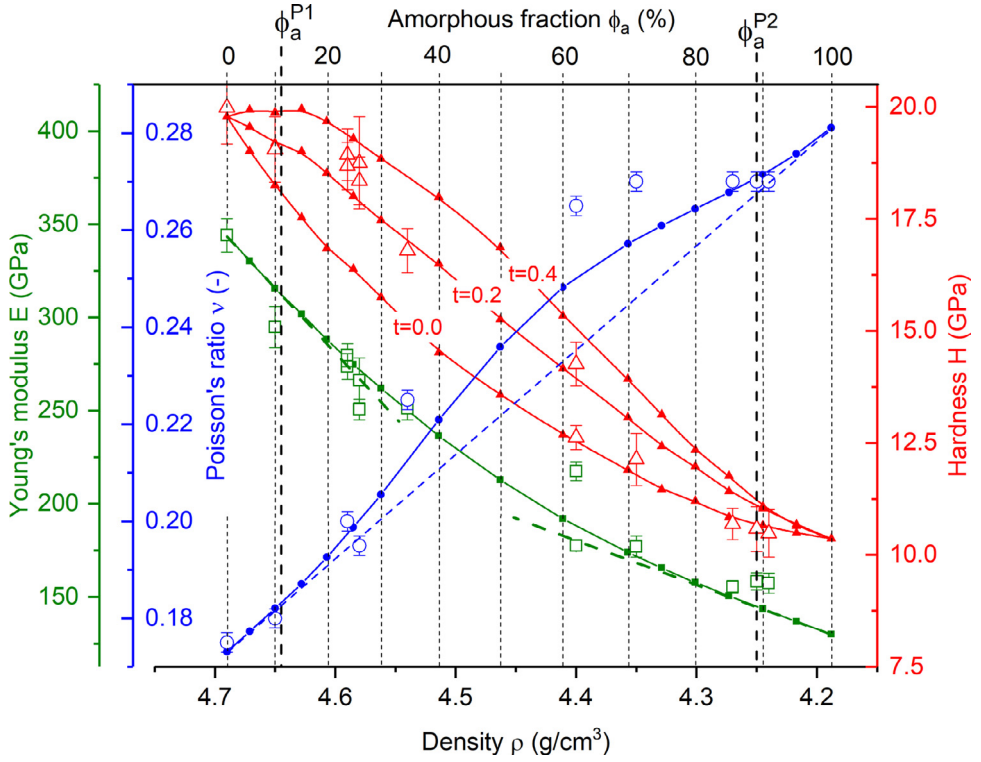

Fig. 4. Predicted mechanical properties (curves with solid symbols) in comparison with experimental data (open symbols) published in [26,27] as function of density. Hardness values H are obtained from the nanoindentation model fed with properties obtained from the micromechanical model without interface ($t = 0.0$) and with an interface of increasing thickness $t = 0.2$ and 0.4. Data are available at [48].

not represent the microstructure of partially amorphized zircon in all aspects. A comparison of both microstructures would require TEM tomography, which would be an interesting direction of future work.

The predicted hardness is plotted in Fig. 4 together with the nanoindentation results from Beirau et al. [26,27] as red curve and open triangles, respectively. The model without an interface between the two phases ($t = 0$) is in good agreement with the nanoindentation data for $\phi_a > 60\%$. For the remaining data, the hardness is considerably increased, particularly for amorphous fractions from 10% to 30%. Beirau et al. [27] discussed this characteristic feature in the hardness in connection with results from NMR measurements [49] and molecular dynamics simulations [50] that show that each recoil cascade in zircon consists of a low density core surrounded by a densified outer layer, populated by SiO_n polymers. As a possible explanation for the observed higher hardness, combined effects of interfaces between crystalline and amorphized regions and underlying hard shells of each recoil cascade were identified.

To investigate the effect of such a hard interface in dependence of the amorphous fraction in the spirit of [27], the moduli of zircon are less affected by soft interfaces and hard shells and, therefore, we assume that the macroscopic Young's modulus for $t > 0$ is the same as for $t = 0$. The results with a reinforced interface between the amorphous and crystalline phase are shown in Fig. 4 as red curves, labelled with $t = 0.2$ and 0.4. The curves indicate that the interfacial strengthening in the material is most effective within the two percolation transitions, i.e. when both phases form a bi-continuous microstructure. This leads to a characteristic change in the slope exceeding ϕ_a^{P1}, where the amorphous islands start to connect and form a continuous network. The formed cusp with increasing interface thickness confirms the assumed relation by [27].

In summary, the simulation results show a good agreement with previous experimental data [26,27]. This confirms that the assumptions introduced in the model setup and for natural radiation-damaged zircon are reasonable. Two percolation transitions can be found in the system, occurring with ongoing radiation damage. According to the literature and the model established in this work, microstructures with volumetric percolation points at ~ 16 and $\sim 84\%$ ϕ_a provide a good approximation of the macroscopic behaviour. The Youngś modulus indicates a sensitivity with respect to the corresponding thresholds, while interface effects (including the hard shells) are able to stabilise the hardness relative to the decay without such interfaces, forming a cusp with a maximum around ϕ_a^{P1}. As we have a composite material of two solid phases, one serves as matrix material for the other, as soon as the phase with the lower volume fraction forms disconnected islands. Therefore, the load path still exists while the connectivity within one of the phases is broken. This explains why the mechanical properties change smoothly around the percolation transitions. Consequently, it is almost impossible to determine the exact location of the percolation transitions without a combined experimental-modelling approach, as presented in this work. Further, the good agreement between the numerical results from our model and the experimental results from literature implies that the level-cut Gaussian random field modelling approach is suitable for studying the mechanical effect of nanoporosity, as well as of radiation damage related amorphization. The modelling approach has the potential for predicting the intrinsic radiation damage related evolution of the mechanical properties also for other materials that show similar percolation transitions. Modelling of materials that are exposed to radiation is also possible by extending the model with a density gradient over the depth. This would require additional data, such as the fluence-density relationship and knowledge of the decay of the fluence over the depth.

Funding

This work was supported by the Deutsche Forschungsgemeinschaft (DFG, German Research Foundation) [grant number BE 5456/2-1].

Declaration of Competing Interest

The authors declare that they have no known competing financial interests or personal relationships that could have appeared to influence the work reported in this paper.

Acknowledgement

We like to thank W.D. Nix (Stanford University) for helpful comments on an earlier version of this manuscript.

References

[1] R.C. Ewing, R.F. Haaker, Nucl. Chem. Waste Manage. 1 (1980) 51–57.
[2] R.C. Ewing, B.C. Chakoumakos, G.R. Lumpkin, T. Murakami, R.B. Greegor, F.W. Lytle, Nucl. Instrum. Methods Phys. Res. B 32 (1988) 487–497.
[3] C. Keller, Nukleonik 5 (1963) 41–47.
[4] K.H. Walter, Ternäre Oxide des drei- bis- sechswertigen Americiums, Kernforschungszentrum Karlsruhe, Gesellschaft für Kernforschung M.B.H., Karlsruhe, 1965.
[5] J.A. Speer, The actinide orthosilicates, in: P.H. Ribbe (Ed.), Reviews in Mineralogy and Geochemistry, Orthosilicates, 5, Mineralogical Society of America, Chantilly, VA, 1980, pp. 113–135.
[6] J.A. Speer, B.J. Cooper, Am. Mineral. 67 (1982) 804–808.
[7] W.J. Weber, J. Mater. Res. 5 (1990) 2687–2697.
[8] W.J. Weber, Radiat. Eff. Defects Solids 115 (1991) 341–349.
[9] W.J. Weber, J. Am. Ceram. Soc. 76 (1993) 1729–1738.
[10] R.C. Ewing, W. Lutze, W.J. Weber, J. Mater. Res. 10 (1995) 243–246.
[11] E.B. Anderson, B.E. Burakov, E.M. Pazukhin, Radiochim. Acta 60 (1993) 149–151.
[12] B.E. Burakov, in: Proc. Int. Conf. SAFE WASTE, 93, 1993, pp. 19–33.
[13] W.A. Deer, R.A. Howie, J. Zussman, Rock Forming Minerals: Orthosilicates, The Geological Society, London, 1997.
[14] B.E. Burakov, J.M. Hanchar, M.V. Zamoryanskaya, V.M. Garbuzov, V.A. Zirlin, Radiochim. Acta 90 (2002) 95–97.
[15] W.J. Weber, R.C. Ewing, A. Meldrum, J. Nucl. Mater. 250 (1997) 147–155.
[16] R.C. Ewing, Proc. Natl. Acad. Sci. U. S. A. 96 (1999) 3432–3439.
[17] R.C. Ewing, Prog. Nucl. Energy 49 (2007) 635–643.
[18] S. Szenknect, D. Alby, M. López García, C. Wang, R. Podor, F. Miserque, A. Mesbah, L. Duro, L. Zetterström Evins, N. Dacheux, J. Bruno, R.C. Ewing, Sci. Rep. 10 (2020) 12168.
[19] T. Murakami, B.C. Chakoumakos, R.C. Ewing, G.R. Lumpkin, W.J. Weber, Am. Mineral. 76 (1991) 1510–1532.
[20] R.C. Ewing, Nature 445 (2007) 161–162.
[21] R.C. Ewing, Mineral. Mag. 75 (2011) 2359–2377.
[22] I. Farnan, H. Cho, W.J. Weber, Nature 445 (2007) 190–193.
[23] K. Trachenko, M.T. Dove, E.K.H. Salje, J. Phys. 15 (2003) L1–L7.
[24] H.D. Holland, D. Gottfried, Acta Cryst. 8 (1955) 291–300.
[25] B.C. Chakoumakos, W.C. Oliver, G.R. Lumpkin, R.C. Ewing, Radiat. Eff. Defects Solids 118 (1991) 393–403.
[26] T. Beirau, W.D. Nix, U. Bismayer, L.A. Boatner, S.G. Isaacson, R.C. Ewing, Phys. Chem. Miner. 43 (2016) 627–638.
[27] T. Beirau, W.D. Nix, R.C. Ewing, H. Pöllmann, E.K.H. Salje, Appl. Phys. Lett. 112 (2018) 201901.
[28] A.P. Roberts, E.J. Garboczi, Proc. R. Soc. Lond. A 458 (2002) 1033–1054.
[29] C. Soyarslan, S. Bargmann, M. Pradas, J. Weissmüller, Acta Mater. 149 (2018) 326–340.
[30] J.W. Cahn, J. Chem. Phys. 42 (1965) 93–99.
[31] A.P. Roberts, E.J. Garboczi, J. Mech. Phys. Solids 47 (1999) 2029–2055.
[32] E.K.H. Salje, J. Chrosch, R.C. Ewing, Am. Mineral. 84 (1999) 1107–1116.
[33] K. Trachenko, M.T. Dove, E. Salje, J. Appl. Phys. 87 (2000) 7702–7707.
[34] T. Beirau, W.C. Oliver, C.E. Reissner, W.D. Nix, H. Pöllmann, R.C. Ewing, Appl. Phys. Lett. 115 (2019) 81902.
[35] H. Scher, R. Zallen, J. Chem. Phys. 53 (1970) 3759–3761.
[36] S. Ríos, E.K.H. Salje, M. Zhang, R.C. Ewing, J. Phys. 12 (2000) 2401–2412.
[37] M. Zhang, E.K.H. Salje, J. Phys. 13 (2001) 3057–3071.
[38] S. Rıós, E.K.H. Salje, Appl. Phys. Lett. 84 (2004) 2061–2063.
[39] W.J. Weber, R.C. Ewing, L.-M. Wang, J. Mater. Res. 9 (1994) 688–698.
[40] S. Ríos, T. Malcherek, E.K.H. Salje, C. Domeneghetti, Acta Cryst. B 56 (Pt 6) (2000) 947–952.
[41] Abaqus, 3DEXPERIENCE, Dassault Systemes SIMULIA Corp., Johnston, RI, USA, 2020.
[42] N. Huber, W.D. Nix, H. Gao, Proc. R. Soc. Lond. A 458 (2002) 1593–1620.
[43] J. Yu, R. Devanathan, W.J. Weber, J. Mater. Chem. 19 (2009) 3923–3930.

[44] A. Diver, O. Dicks, A.M. Elena, I.T. Todorov, K. Trachenko, J. Phys. 32 (2020) 415703.
[45] R.K. Eby, R.C. Ewing, R.C. Birtcher, J. Mater. Res. 7 (1992) 3080–3102.
[46] N.M.A. Krishnan, R. Ravinder, R. Kumar, Y. Le Pape, G. Sant, M. Bauchy, Acta Mater. 166 (2019) 611–617.
[47] A. Stukowski, Modell. Simul. Mater. Sci. Eng. 18 (2010) 15012 [dataset].
[48] N. Huber, T. Beirau, Mechanical Properties of Zircon for Varying Degree of Amorphization Predicted by Finite Element Simulations, TUHH Universitätsbibliothek, 2020, doi:10.15480/336.2879.
[49] I. Farnan, E.K.H. Salje, J. Appl. Phys. 89 (2001) 2084–2090.
[50] K. Trachenko, M.T. Dove, E.K.H. Salje, Phys. Rev. B 65 (2002) 180102(R).